Available online at www.sciencedirect.com
SCIENCE DIRECT
Microporous and Mesoporous Materials 91 (2006) 225–232
MICROPOROUS AND MESOPOROUS MATERIALS
www.elsevier.com/locate/micromeso

Synthesis of ordered mesoporous Zr–P–Al materials with high thermal stability

Ziyu Liu, Yingxu Wei, Yue Qi, Xianbin Liu, Yinfeng Zhao, Zhongmin Liu *

Applied Catalysis Laboratory, Dalian Institute of Chemical Physics, Chinese Academy of Sciences, 457 Zhongshan Road, Dalian 116023, PR China

Received 14 November 2005; received in revised form 21 November 2005; accepted 23 November 2005
Available online 18 January 2006

Abstract

A kind of mesoporous Zr–P–Al materials was synthesized by a three-step method, in which a hexagonal zirconium oxide–sulfate composite was prepared and subsequently treated with a phosphoric acid solution followed by the treatment with $AlCl_3$ solutions. These materials had ordered cylindrical pores, and their textual data depended on the amount of $AlCl_3$ and calcination temperature. Small amount of Al incorporation (Al/Zr = 0.49) leaded to a microporous material with a Brunauer–Emmett–Teller (BET) specific surface area of 314 m^2/g and a pore size of 0.6 nm. Increasing the Al/Zr ratio resulted in mesoporous materials with higher BET specific surface area. The mesoporous Zr–P–Al material exhibited a BET specific surface area of 462 m^2/g and a pore size of 2.9 nm after calcination at 773 K. 973 K calcination led to a BET specific surface area of 416 m^2/g and a pore size of 2.7 nm. Even after calcination at 1073 K, a BET specific surface area of 227 m^2/g and a pore size of 3.2 nm could still be observed. The pentacoordinated aluminium species seemed to be indispensable for the synthesis of mesoporous Zr–P–Al materials because of their effective reduction of the lattice contraction. NMR results showed that a hexacoordinated aluminium layer, a $(HO)_2P(O–Zr)_2$ layer and a Zr(OH) layer combined with each other were formed after $AlCl_3$ treatment. Upon calcination, the layers of Al_2O_3, $(Zr–O)_2PO_2$ and ZrO_2 formed the walls of the mesoporous Zr–P–Al materials. This unique structure was suggested to be responsible for the high thermal stability (up to 1073 K).

Keywords: Mesoporous; Zr–P–Al materials; Post-synthetic treatment; Thermal stability

1. Introduction

Non-siliceous mesoporous materials have been studied a great lot over the last decade for their potential applications as heterogeneous catalysts and sorbents [1]. Mesoporous zirconium oxide seems to be the most attractive non-siliceous mesoporous materials since crystalline ZrO_2 has been used extensively in chemical and petrochemical processes [2,3]. Much effort has been devoted to the synthesis of mesoporous zirconium oxides [4–13]. However, most of these mesostructures collapsed after removal of the surfactant through calcination, with only few exceptions. Knowles et al. [9,10] prepared the first thermally stable mesoporous zirconium oxide after calcination at 773 K. Yang et al. [11,12] synthesized another through a block copolymer route, which was proved to be stable until 723 K. Recently, Suh et al. [13] reported the synthesis of a mesoporous zirconium oxide by an atrane route and the material remained stable at 773 K.

Several methods have been employed to improve the thermal stability of zirconium oxide mesostructures. One is to use anionic surfactants as the template, such as Na lauryl sulfate and monododecyl phosphate (P_{12}). Fripiat et al. [14–16] reported that the calcination temperature of the resulted mesoporous materials could reach 773 K, but these materials showed disordered pore systems. Another method is to add secondary metal source directly to the gel system. For example, binary Ti–Zr [17], Y–Zr [18,19], Ce–Zr [19] and Sn–Zr [20] mesoporous materials were reported to be stable also to 773 K. Besides these two

* Corresponding author. Tel.: +86 411 84685510; fax: +86 411 84691570.
E-mail address: Liuzm@dicp.ac.cn (Z. Liu).

1387-1811/$ - see front matter © 2005 Elsevier Inc. All rights reserved.
doi:10.1016/j.micromeso.2005.11.050

methods, treating the uncalcined zirconium oxide in Na_2CrO_4 [21], $NH_3 \cdot H_2O$ [22], H_2SO_4 [23] or H_3PO_4 solutions [24–32] was effective to improve the thermal stability. With post-synthetic treatment with H_3PO_4 solution, the obtained Zr–P materials retained ordered up to 773–873 K [27–32]. However, even with these improvements, the strong lattice contractions of 31% [27] or 27% [30] upon 773 K calcination transferred the Zr–P to microporous materials, which restricted their applications in reactions where mesopores are needed. Synthesis of zirconium oxide-based materials with well-ordered mesopores and thermal stability higher than 773 K is still difficult and merits further effort. The work in the field of mesoporous metal–Zr–Y materials provided a possible way for synthesizing thermally stable trinary materials [33,34]. This also predicts a possible way to reduce the lattice contraction and preserve the mesopores of Zr–P by adding a third element after calcination. Taking into account of the well-known interaction between P and Al, element Al is the appropriate candidate. The thermal stability enhancement for Zr–S materials by the Al incorporation had already been proved [35], but adding Al source directly to the zirconium containing gel system resulted in only disordered pore systems.

In this study, we try to synthesize a kind of ordered mesoporous Zr–P–Al materials with enhanced thermal stability by a three-step method, in which a hexagonal zirconium oxide–sulfate composite is prepared and subsequently treated with a phosphoric acid solution followed by the treatment with $AlCl_3$ solutions. The textual properties of these materials are characterized and the thermal stability is investigated in detail. A possible scheme for the formation of these structures is also presented.

2. Experimental

2.1. Synthesis

A mixture of hexadecyltrimethylammonium bromide (CTAB) and $Zr(SO_4)_2 \cdot 4H_2O$ was dispersed in deionized water with a molar composition of $Zr(SO_4)_2$:CTAB:H_2O = 1:0.27:240. After being stirred at 353 K for 2 h, the resulting suspension was crystallized at 373 K for 48 h. The precipitate was centrifuged, washed with deionized water and dried at 373 K. The resulting sample was designated as MZ. Subsequently, 10 g of MZ was stirred in 200 ml of 0.25 M phosphoric acid solution for 2 h at room temperature. The sample was recovered after being centrifuged and dried, and was designated as MZP. One gram of MZP was stirred in 100 ml of 0.1 M ethylamine solution at ambient temperature for 24 h, then different volume of 0.2 M $AlCl_3 \cdot 6H_2O$ solutions were added to the suspension, and finally, 0.2 M NaOH was slowly dropped in until pH = 4.2. These mixtures were refluxed at 368 K for 24 h, then the solids were separated, washed and dried to form the Zr–P–Al materials, which were denoted as $MZPAl_x$ (x = 0.7–14), where x is the mass ratio of $AlCl_3 \cdot 6H_2O$ to MZP.

Calcinations were carried out in air at given temperatures for 6 h. In order to distinguish the samples calcined or not, we used the compound expression "as-synthesized" to refer to the samples containing CTAB and without calcinations, as has been used extensively in the field of material synthesis.

2.2. Characterization

Powder X-ray diffraction (XRD) patterns were recorded on a D/Max-b X-ray diffractometer with CuKα radiation. Chemical compositions were obtained by X-ray fluorescence (XRF) method on a Philips Magix X spectrometer. Fourier transform infrared spectroscopy (FTIR) studies were performed on a Bruker EQUINOX 55 spectrometer by KBr pellet method. Transmission electron microscopy (TEM) studies were carried out with a JEOL JEM-2000Ex electron microscope. The textural data were obtained by nitrogen adsorption measurement using a Micromeritics 2010 BET analyzer. Prior to the measurements, the samples were outgassed at 623 K for at least 4 h. Solid-state ^{31}P MAS NMR spectra were obtained on a Varian InfinityPlus 400 spectrometer equipped with a 5 mm zirconia rotor (6 kHz spin rate) operating at 161.97 MHz and 8.0 s of pulse delay with a spectral width of 50.0 kHz. Solid-state ^{27}Al MAS NMR spectra were obtained on a Varian InfinityPlus 300 spectrometer equipped with a 4 mm zirconia rotor (12 kHz spin rate) operating at 78.12 MHz and 8.0 s of pulse delay with a spectral width of 50.0 kHz. The chemical shifts of ^{31}P and ^{27}Al (in ppm) were externally referenced to 85% H_3PO_4 and $[Al(H_2O)_6]^{3+}$ aqueous solutions, respectively.

3. Results and discussion

As shown in Fig. 1, all the XRD patterns of the as-synthesized samples exhibit diffraction peaks in low angle region, indicating the mesostructural property. MZ shows three characteristic diffraction peaks corresponding to d spacings of 4.19, 2.40 and 2.09 nm (Fig. 1A), which are similar to those reported previously and are indexed as (100), (110) and (200) of a hexagonal mesostructure with a lattice constant a_0 of 4.84 nm ($a_0 = 2d_{(100)}/\sqrt{3}$) [27]. After the phosphoric acid treatment, the hexagonal structure retains completely and the pore array becomes even more ordered (Fig. 1B). A slight increase in the intensity of the (100) diffraction is also observed. The a_0 of MZP is almost the same as that of MZ (Table 1), which is different from the report of Ciesla et al. [27], who obtained an enlarged a_0 with H_3PO_4 treatment. After treating MZP with $AlCl_3$, the intensities of (100) peaks change little from $MZPAl_{0.7}$ to $MZPAl_7$ (Fig. 1C–E) but that of $MZPAl_{14}$ is enhanced greatly (Fig. 1F). Compared to that of MZP, the a_0 of $MZPAl_{0.7}$ reduces a little as indicated by the (100) diffraction shifting to higher angles, while the a_0 of $MZPAl_x$ increases with the increase of x value.

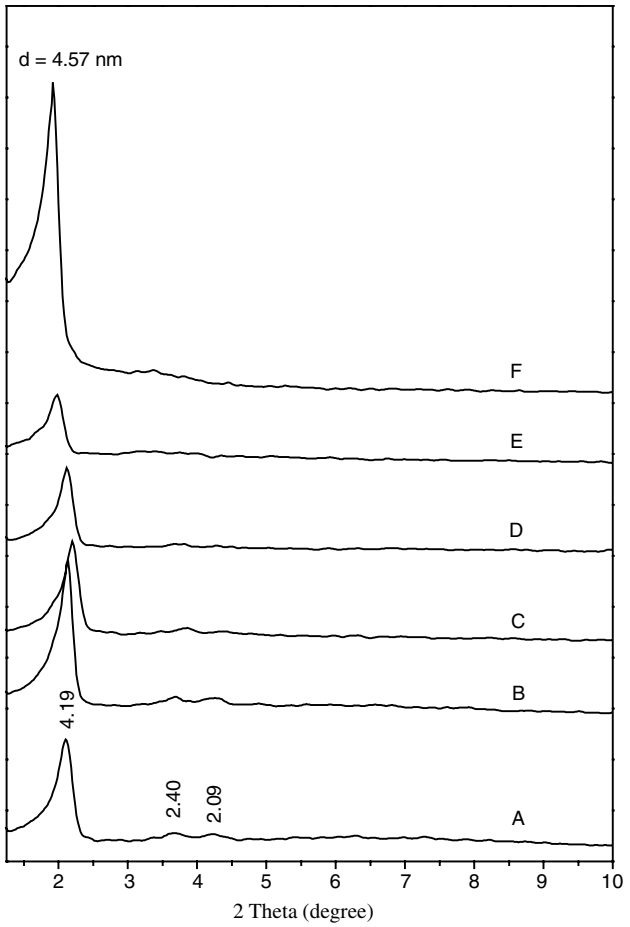

Fig. 1. XRD patterns of as-synthesized (A) MZ, (B) MZP, (C) $MZPAl_{0.7}$, (D) $MZPAl_{1.8}$, (E) $MZPAl_7$ and (F) $MZPAl_{14}$.

Table 1
Molar ratios of $MZPAl_x$ calculated from XRF results and structure parameters from XRD patterns

Sample	S/Zr ratio	P/Zr ratio	Al/Zr ratio	$d_{(100)}$ (nm)	a_0 (nm)
MZ	0.92	–[a]	–[a]	4.19	4.84
MZP	0.29	0.53	–[a]	4.14	4.78
$MZPAl_{0.7}$	0.20	0.66	0.49	4.01	4.63
$MZPAl_{1.8}$	0.22	0.86	1.57	4.16	4.80
$MZPAl_7$	0.34	1.06	2.57	4.46	5.15
$MZPAl_{14}$	0.35	1.49	3.16	4.57	5.28

[a] No P or Al could be detected.

Table 1 shows that for MZ sample only S and Zr can be detected and the ratio of S/Zr is 0.92. Once MZ is treated by H_3PO_4, the S/Zr ratio decreases to 0.29 and P/Zr ratio increases to 0.53 for MZP, indicating that sulfate species have been replaced partly by phosphate species for their difference in complexing ability ($\alpha = 50\%$ for Zr–P and $\alpha = 32\%$ for Zr–S) [36]. The existence of part of sulfate species in MZP shows that there is equilibrium between the Zr–S and Zr–P, so a fraction of zirconium is not available to react with H_3PO_4. For Zr–P synthesis, $Zr(SO_4)_2$ and $ZrOCl_2$ were both used as the precursors at the beginning of our study. $ZrOCl_2$ was not as successful a precursor as $Zr(SO_4)_2$, and only amorphous products were obtained from it. In literatures, some mesoporous ZrO_2 have been synthesized from sulphate-free zirconium precursors, such as $ZrCl_4$ [11,12], $Zr(n\text{-}OPr)_4$ [23,37] or $Zr(i\text{-}OPr)$ [7], but no Zr–P materials were reported except those using P_{12} as surfactant, and the Zr–P materials obtained by this way were disordered [15,16]. It is still difficult or even impossible to synthesize ordered Zr–P materials from sulphate-free zirconium precursors up to now. As listed in Table 1, the P/Zr ratio of MZP is far below 2, indicating that part of Zr(OH) may still exist in the sample [30]. After treatments with $AlCl_3$, the S/Zr, P/Zr and Al/Zr ratios all increase from $MZPAl_{0.7}$ to $MZPAl_{14}$. The increase of Al/Zr ratio is caused by the Al incorporation, while the increasing S/Zr and P/Zr ratio demonstrate that some Zr atoms were lost during the $AlCl_3$ treatment since no S and P sources were added at this step. Since the S/Zr ratio changes slightly while phosphate groups do not affect a_0 obviously as mentioned above, the evident a_0 enlargement of $MZPAl_x$ should be related to more Al incorporation.

FTIR spectra of the as-synthesized samples are given in Fig. 2. For MZP sample (Fig. 2A), the broad bands at about 3500 and 1640 cm^{-1} stem from the absorbed water on the surface while the bands centered at 1000–1100 cm^{-1} should be attributed to the stretching vibration of phosphate groups [26,29]. The bands at 3000–2800 and 1477 cm^{-1} that originated from the stretching and deformation vibrations of C–H of surfactant CTAB are also observed. Fig. 2B shows that no obvious changes occur after the ethylamine treatment, implying the still existence of CTAB. When Al is incorporated into MZP (Fig. 2C–E), the bands at 3000–2800 cm^{-1} disappear and the bands at 1477 cm^{-1} weaken greatly for all $MZPAl_x$ samples, indicating that majority of the surfactant has been removed after the post-synthetic treatment with $AlCl_3$. We speculate that the Al^{3+} ions gather between the CTAB micelle and

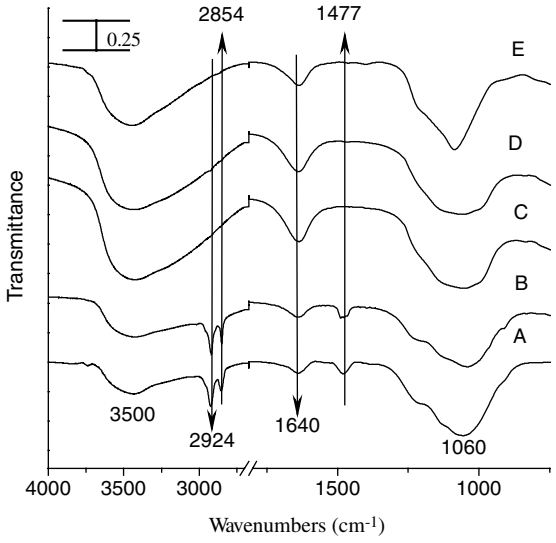

Fig. 2. IR spectra of as-synthesized (A) MZP, (B) ethylamine treated MZP, (C) $MZPAl_{0.7}$, (D) $MZPAl_{1.8}$ and (E) $MZPAl_{14}$.

the P species of MZP. The Al^{3+} will repel the CTA^+ ions because they are much positively charged and have high tendency to react with P species. Thus most of CTAB is removed in this step. Usually, the removal of the surfactant will reduce the a_0 of mesostructures, as in the case of MCM-41 [38]. But no a_0 reduction occurs except $MZPAl_{0.7}$ when compared to MZP (Table 1). In our study, ethylamine solution was used before the $AlCl_3$ treatment, which is effective for a_0 enlargement [39]. In fact the ethylamine treated MZP showed an enlarged a_0 of 5.37 nm. In the subsequent removal of CTAB by the $AlCl_3$ treatment, some contraction of the enlarged a_0 can be observed when less Al was incorporated ($x = 0.7$, 1.8) while the contraction becomes neglectable for $MZPAl_x$ with more Al incorporation ($x = 7$, 14). The $AlCl_3$ treatment reduces the contraction, which accounts for the a_0 enlargement of $MZPAl_x$.

Fig. 3 shows typical TEM images of as-synthesized samples. All the samples exhibit arrays of parallel lines, indicating the formation of ordered structures. These parallel lines can be attributed to lamellar structures or cylindrical pores of hexagonal structures. The latter can be confirmed because the ordered structures remain even after calcination at 773 K, as discussed below, while lamellar structures usually collapse at 623 K [40]. The a_0s measured from TEM are 4.5, 4.2, 4.3 and 4.7 nm for MZP (Fig. 3A), $MZPAl_{0.7}$ (Fig. 3B), $MZPAl_{1.8}$ (Fig. 3C) and $MZPAl_{14}$ (Fig. 3D), respectively. These results are in agreement with those detected from XRD.

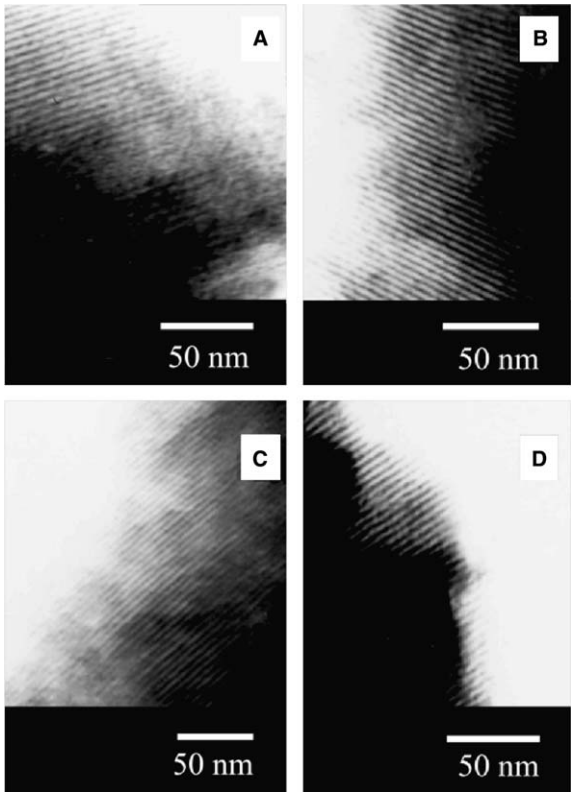

Fig. 3. TEM images of as-synthesized (A) MZP, (B) $MZPAl_{0.7}$, (C) $MZPAl_{1.8}$ and (D) $MZPAl_{14}$.

The samples were calcined at 773 K to remove the surfactant completely. All samples remained the (1 0 0) reflections, implying the presence of ordered structures. The a_0s of the calcined samples are listed in Table 2. Compared with those in Table 1, all the a_0s are reduced indicating that some lattice contractions occur after calcination. The contraction of MZP is 23%, while the contraction of $MZPAl_{0.7–14}$ is 15%, 4%, 9% and 8%, respectively, which means that the $AlCl_3$ treatment reduces the lattice contractions and mesopores may form in this way.

Fig. 4 depicts the effect of $AlCl_3 \cdot 6H_2O$/MZP ratios (x values) on the textural properties of 773 K calcined samples. Obviously, the mesostructure of MZP collapses after calcination (Fig. 4A), as confirmed by the extremely low BET specific surface area of 8 m^2/g in Table 2. After the $AlCl_3$ treatment, $MZPAl_{0.7}$ shows an isotherm similar to *type I* (Fig. 4B), indicating a microporous structure. The BET specific surface area increases sharply to 314 m^2/g and the pore size distribution is centred at 0.6 nm. This proves that even small amount of Al incorporation (Al/Zr = 0.49, Table 1) can enhance the thermal stability of Zr–P. Increasing the x value to 1.8 results in a *type IV* isotherm (Fig. 4C), with a strong uptake of N_2 in a relative pressure (p/p_0) range of 0.2–0.4 due to capillary condensation predicting the formation of mesoporous structure. The adsorption at lower

Table 2
Textural data for calcined MZP and $MZPAl_x$

Sample	Calcination temperature (K)	BET specific surface area (m^2/g)	Pore volume (cm^3/g)	Pore size (nm)	$d_{(100)}$ (nm)	a_0 (nm)	Wall thickness* (nm)
MZP	773	8	–[a]	–[a]	3.17	3.66	–[a]
$MZPAl_{0.7}$	773	314	0.09	0.6	3.41	3.94	3.34
$MZPAl_{1.8}$	773	393	0.21	2.8	3.98	4.60	1.80
$MZPAl_7$	773	453	0.34	2.9	4.04	4.67	1.77
$MZPAl_{14}$	773	462	0.36	2.9	4.24	4.90	2.00
$MZPAl_{14}$	873	412	0.34	3.0	4.07	4.70	1.70
$MZPAl_{14}$	973	416	0.31	2.7	3.92	4.53	1.83
$MZPAl_{14}$	1073	227	0.16	3.2	3.68	4.25	1.05
$MZPAl_{14}$	1173	10	–[a]	–[a]	T[b]	T[b]	–[a]

[a] No mesoporosity could be detected.
[b] Tetragonal phase.
* Wall thickness = a_0 − pore size.

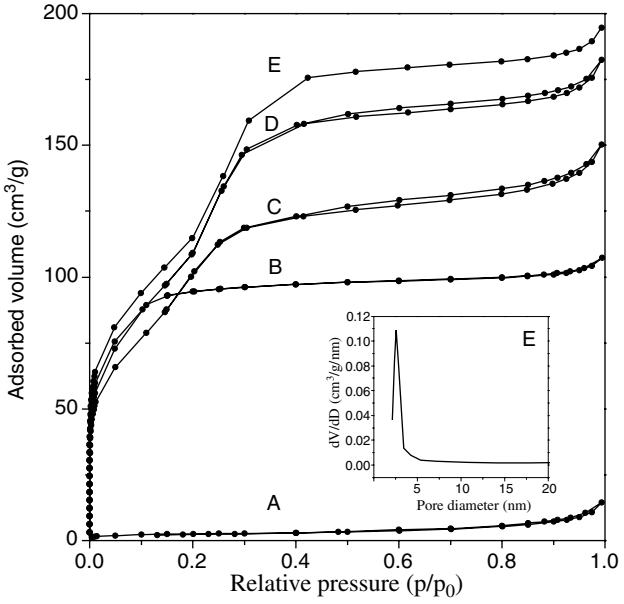

Fig. 4. N_2 adsorption isotherms of samples calcined at 773 K: (A) MZP, (B) $MZPAl_{0.7}$, (C) $MZPAl_{1.8}$, (D) $MZPAl_7$ and (E) $MZPAl_{14}$. Inset is the pore size distribution of (E).

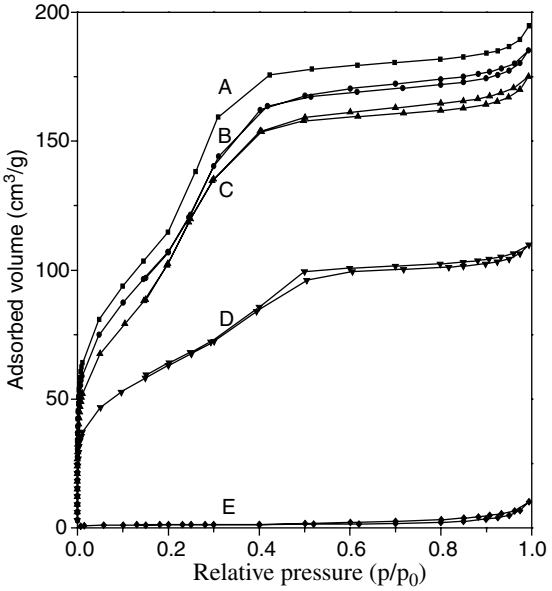

Fig. 5. N_2 adsorption isotherms of $MZPAl_{14}$ after calcination at (A) 773 K, (B) 873 K, (C) 973 K, (D) 1073 K and (E) 1173 K.

p/p_0 (~60 cm^3/g) is most probably due to the monolayer coverage of the walls and not from the micropores [41]. The sample exhibits a BET specific surface area of 393 m^2/g, a pore volume of 0.21 cm^3/g and a pore size of 2.8 nm. Further increasing to $x = 7$ also results in a *type IV* isotherm from a mesoporous structure (Fig. 4D), but with even higher BET specific surface area, pore volume and appreciably bigger pore size. $MZPAl_{14}$ exhibits a BET specific surface area of 462 m^2/g and a pore volume of 0.36 cm^3/g (Fig. 4E and Table 2), which are higher than most of the Zr–P materials [13,27–31]. The uniform pore size distribution of this sample is centred at 2.9 nm (Fig. 4 Inset). The textural data verify that $AlCl_3$ treatment contributes to the porosity and enhances the thermal stability of the Zr–P material. The pore size of these resulting Zr–P–Al materials can be changed from microporous ($x = 0.7$) to mesoporous ($x = 1.8$–14) by adjusting the amount of incorporated Al. As for the mesoporous ones, the almost unchanged pore size may be related to the increasing a_0 and the increasing wall thickness.

Calcination in temperature range of 773–1173 K was performed over $MZPAl_{14}$ to text its thermal stability at higher temperatures, and N_2 adsorption isotherms of these calcined samples are given in Fig. 5. Similar *type IV* isotherms can be observed for samples calcined at 773–1073 K, but their BET specific surface area and pore volume decrease gradually with temperature increases (Table 2). The losses of the mesoporous structure are neglectable below 973 K but are accelerated from then on. 973 K calcination led to a BET specific surface area of 416 m^2/g and a pore size of 2.7 nm, while a BET specific surface area of 227 m^2/g and a pore size distribution of 3.2 nm are obtained after calcination at 1073 K. The pore size of these materials increases with the increasing temperature from 773 K to 1073 K. This may be related to the lowered wall thickness. As shown in Table 2, the wall thickness of calcined $MZPAl_{14}$ decreases from 2.00 to 1.05 nm, meanwhile, the pore size increases from 2.9 to 3.2 nm. Increasing the calcination temperature to 1173 K, however, leads to an extremely low BET specific surface area. XRD patterns showed that the mesostructure had collapsed and a tetragonal phase was obtained.

^{27}Al and ^{31}P MAS NMR spectra of some samples are shown in Fig. 6. In all the ^{27}Al MAS NMR spectra, no resonances at range of 38–45 ppm can be found, so the existence of tetrahedral aluminium as that in microporous $AlPO_4$ can be excluded [42]. The Al species might just react with surface P species of Zr–P and did not enter the Zr–P pore walls. $MZPAl_{0.7}$ displays one resonance at about −2.0 ppm (Fig. 6a(A)), which can be assigned to hexacoordinated aluminium [14,43]. For the sample of $MZPAl_{1.8}$, besides the resonance of hexacoordinated aluminium, a new resonance at about 31 ppm appears in the spectrum (Fig. 6a(B)), which can be attributed to the pentacoordinated aluminium [43,44]. $MZPAl_{14}$ also shows these two resonances, but their intensities are increased (Fig. 6a(C)). In a previous study where layered α-zirconium phosphate was pillared by alumina [45], similar penta- and hexacoordinated aluminium species were also reported. It was further suggested that the linkage between the phosphate layers and Al ions was established through the pentacoordinated Al, whereas the hexacoordinated Al formed the pillars between the layers [45,46]. In our study, the pores of $MZPAl_x$s have been proved to be cylindrical by TEM, so we propose that the hexacoordinated aluminium form a layer along the cylindrical pores, which is bonded to the P species through the pentacoordinated aluminium ($x > 0.7$). The absence of

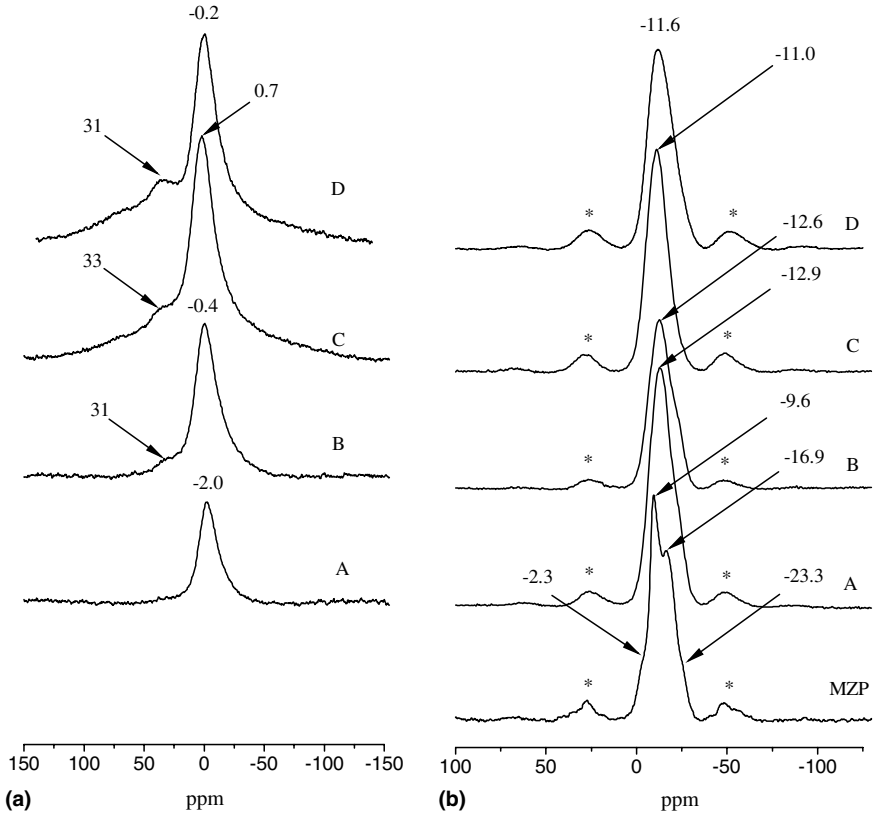

Fig. 6. (a) ^{27}Al and (b) ^{31}P MAS NMR spectra of as-synthesized (A) $MZPAl_{0.7}$, (B) $MZPAl_{1.8}$, (C) $MZPAl_{14}$ and (D) 773 K calcined $MZPAl_{14}$. *Spinning side band (SSB).

the pentacoordinated aluminium species in $MZPAl_{0.7}$ brings about no effective linkage between the hexacoordinated aluminium and the P species. It may be the reason why this sample shows the largest lattice contraction in $MZPAl_x$s and turned to microporous after calcination. So in the present study the formation of pentacoordinated aluminium species seems to be indispensable for the synthesis of mesoporous Zr–P–Al materials. Fig. 6a also shows that most of the Al incorporated is hexacoordinated, and its amount increases with the increasing $AlCl_3 \cdot 6H_2O$/MZP ratio. This may thicken the hexacoordinated aluminium layers and thus increase the wall thickness, which is confirmed by the data in Table 2, where the wall thickness increases from 1.8 to 2.0 nm for $MZPAl_{1.8–14}$. After calcination, the increase in the amount of pentacoordinated aluminium species of $MZPAl_{14}$ shows that Al reacts progressively with MZP during calcination (Fig. 6a(D)).

The ^{31}P MAS NMR spectrum of MZP shows four resonances centred at −2.3, −9.6, −16.9 and −23.3 ppm, which can be attributed to $(HO)_3PO–Zr$, $(HO)_2P(O–Zr)_2$, $HOP(O–Zr)_3$ and $P(O–Zr)_4$ according to literature [24], respectively. However, only one resonance appears at −10.9 to −12.9 ppm for each $MZPAl_x$ (Fig. 6b(A–C)), which can be assigned to $(HO)_2P(O–Zr)_2$. Compared to that of MZP, the chemical shifts of $(HO)_2P(O–Zr)_2$ for $MZPAl_x$s appear at relatively higher field, which may be caused by the interaction between the phosphate groups and the Al species [46]. No resonances at range of −19 to −30 ppm can be detected for $MZPAl_x$s, indicating that the P chemical environments of our samples are different from those of the microporous $AlPO_4$-type materials [47]. It can be inferred that a $(HO)_2P(O–Zr)_2$ layer forms and the layer is bonded to a Zr(OH) layer [30]. Taking into account of the results from ^{27}Al MAS NMR, it is clear that the $(HO)_2P(O–Zr)_2$ layer is also bonded to the hexacoordinated aluminium layer through the pentacoordinated Al ($x > 0.7$). After calcination at 773 K, the ^{31}P spectrum of $MZPAl_{14}$ (Fig. 6b(D)) shifts slightly to higher field compared with that of the as-synthesized one. This stems from the different P species before and after calcination. With calcination, the $(HO)_2P(O–Zr)_2$ layer is turned to a $(Zr–O)_2PO_2$ layer.

A scheme was proposed by Liu et al. [30] for the formation of microporous Zr–P materials, in which a hexagonal ZrS–surf composite was first prepared; and then a layer made up of $(Zr–O)PO_3$ and $(Zr–O)_2PO_2$ was formed during the subsequent H_3PO_4 treatment; finally, a layer of $(Zr–O)_3PO$ and P–O–P was resulted to compose the inorganic wall of Zr–P upon calcination. In the present study, we also started from a hexagonal ZrS–surf composite, but the P species in MZP were somewhat different from those of Liu et al., and a third step composed of ethylamine and $AlCl_3$ treatments was added during the post-synthetic treatment. The synthesis of porous Zr–P–Al materials is illustrated in Scheme 1. In the first step, hexagonal MZ (ZrS–surf)

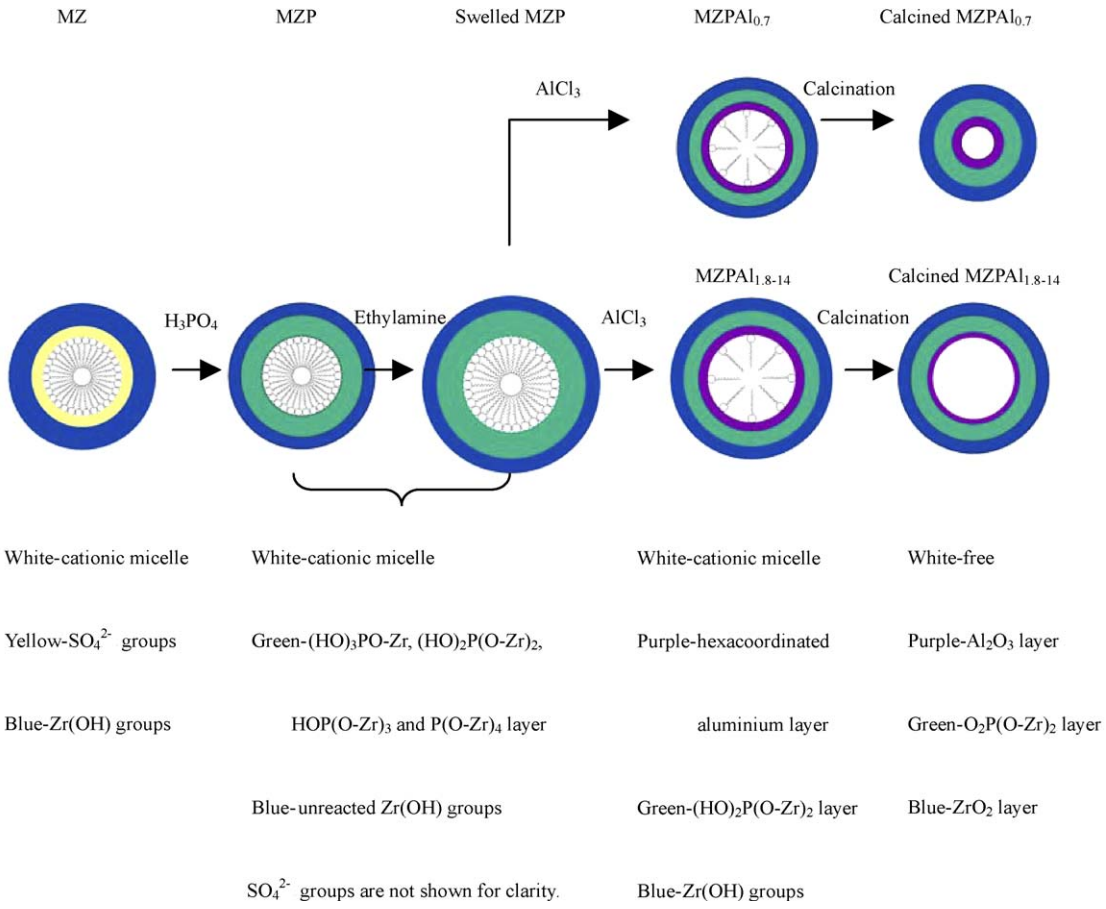

Scheme 1. Synthesis of porous Zr–P–Al materials.

composite was also produced by surfactant-assisted method. In the second step, sulfate species were replaced partly by phosphate species with H_3PO_4 treatment and MZP formed. Meanwhile, the a_0 kept almost unchanged. In the third step, MZP was swelled by the ethylamine treatment, then the subsequent $AlCl_3$ treatment removed most of the surfactant, and the a_0 of $MZPAl_x$ increased with the more Al incorporation. At the same time, a layer of hexacoordinated aluminium species was formed, which was linked to $(HO)_2P(O–Zr)_2$ through pentacoordinated aluminium species ($x > 0.7$). After calcination, the sample with the least Al incorporation ($x = 0.7$) became microporous while the samples with more Al kept the mesoporous structures. Simultaneously, the hexacoordinated aluminium species were transformed to a Al_2O_3 layer, the $(HO)_2P(O–Zr)_2$ to a $(Zr–O)_2PO_2$ layer and the Zr(OH) to a ZrO_2 layer. Thus a complex with layered structures in nanoscale dimension was formed. The pore walls of the Zr–P–Al materials contained layers of Al_2O_3, $(Zr–O)_2PO_2$ and ZrO_2, which were combined with each other. The entire Zr–P–Al material was composed of this kind of three-layered structure units.

4. Conclusions

Mesoporous Zr–P–Al materials with thermal stability up to 1073 K and ordered pore systems were synthesized by a three-step method. A high BET specific surface area of 462 m^2/g and a uniform pore size of 2.9 nm were obtained after calcination at 773 K. Even after calcination at as high as 1073 K, the material still retained mesoporous structure and showed a BET specific surface area of 227 m^2/g and a pore size of 3.2 nm. The amount of Al incorporation affected the textual properties, such as the pore size and BET specific surface area. The formation of a aluminium layer reduced the pore contraction after removal of surfactant, thus the mesopores could be preserved after calcination. The study of NMR indicated that Al species with only hexacoordination state was not enough to keep the material in mesoporous range. Pentacoordinated aluminium species, which were thought to be the effective linkage between the P–Zr and the Al layers, were necessary for the synthesis of thermally stable mesoporous Zr–P–Al materials.

References

[1] F. Schüch, Chem. Mater. 13 (2001) 3184.
[2] Y. Nakano, T. Lizuka, H. Hattori, K. Tanabe, J. Catal. 57 (1979) 1.
[3] K. Tanabe, T. Yamaguchi, Catal. Today 20 (1994) 185.
[4] A. Kim, P. Bruinsma, Y. Chen, L.Q. Wang, J. Liu, Chem. Commun. 2 (1997) 161.
[5] Y.Y. Huang, W.M.H. Sachtler, Chem. Commun. 13 (1997) 1181.
[6] Y.W. Suh, J.W. Lee, H.K. Rhee, Stud. Surf. Sci. Catal. 146 (2003) 235.

[7] M.S. Wong, J.Y. Ying, Chem. Mater. 10 (1998) 2067.
[8] V.I. Pârvulescu, H. Bonnemann, V. Pârvulescu, U. Endruschat, A. Rufinska, Ch.W. Lehmann, B. Tesche, G. Poncelet, Appl. Catal. A: Gen. 214 (2001) 273.
[9] J.A. Knowles, M.J. Hudson, J. Chem. Soc. Chem. Commun. 20 (1995) 2083.
[10] M.J. Hudson, J.A. Knowles, J. Mater. Chem. 6 (1996) 89.
[11] P.D. Yang, D.Y. Zhao, D.I. Margolese, B.F. Chmelka, G.D. Stucky, Nature 396 (1998) 152.
[12] P.D. Yang, D.Y. Zhao, D.I. Margolese, B.F. Chmelka, G.D. Stucky, Chem. Mater. 11 (1999) 2813.
[13] Y.W. Suh, J.W. Lee, H.K. Rhee, Solid State Sci. 5 (2003) 995.
[14] E. Zhao, S.E. Hardcastle, G. Pacheco, A. Garcia, A.L. Blumenfeld, J.J. Fripiat, Micropor. Mesopor. Mater. 31 (1999) 9.
[15] G. Pacheco, E. Zhao, A. Garcia, A. Sklyarov, J.J. Fripiat, Chem. Commun. 5 (1997) 491.
[16] G. Pacheco, E. Zhao, A. Garcia, A. Sklyarov, J.J. Fripiat, J. Mater. Chem. 8 (1998) 219.
[17] H.R. Chen, J.L. Shi, J. Yu, L.Z. Wang, D.S. Yan, Micropor. Mesopor. Mater. 39 (2000) 171.
[18] M. Mamak, N. Coombs, G.A. Ozin, Chem. Commun. 20 (2002) 2300.
[19] E.L. Crepaldi, G.J.de A.A. Soler-Illia, A. Bouchara, D. Grosso, D. Durand, C. Sanchez, Angew. Chem. Int. Ed. 42 (2003) 347.
[20] H.X. Ma, Y. Kong, W.H. Hou, Q.J. Yan, Micropor. Mesopor. Mater. 77 (2005) 241.
[21] J.M. Kim, C.H. Shin, R. Ryoo, Catal. Today 38 (1997) 221.
[22] K. Cassiers, T. Linssen, K. Aerts, P. Cool, O. Lebedev, G.V. Tendeloo, R.V. Grieken, E.F. Vansant, J. Mater. Chem. 13 (2003) 3033.
[23] Y.Y. Huang, T.J. McCarthy, W.M.H. Sachtler, Appl. Catal. A 148 (1996) 135.
[24] S.D. Shen, B.Z. Tian, C.Z. Yu, S.H. Xie, Z.D. Zhang, B. Tu, D.Y. Zhao, Chem. Mater. 15 (2003) 4046.
[25] F. Kleitz, S.J. Thomson, Z. Liu, O. Terasaki, F. Schüth, Chem. Mater. 14 (2002) 4134.
[26] F. Kleitz, S.J. Thomson, Z. Liu, O. Terasaki, F. Schüch, Stud. Surf. Sci. Catal. 146 (2003) 221.
[27] U. Ciesla, S. Schacht, G.D. Stucky, K.K. Unger, F. Schüth, Angew. Chem. Int. Ed. Engl. 35 (1996) 541.
[28] U. Ciesla, M. Fröba, G.D. Stucky, F. Schüth, Chem. Mater. 11 (1999) 227.
[29] H.R. Chen, J.L. Shi, W.H. Zhang, D.S. Yan, J. Inorg. Mater. 15 (2000) 1123.
[30] W. Liu, Z.X. Song, T. Ikegawa, H. Nishiguchi, T. Ishihara, Y. Takita, Mater. Lett. 58 (2004) 3328.
[31] H.R. Chen, J.L. Shi, Z.L. Hua, M.L. Ruan, D.S. Yan, Mater. Lett. 51 (2001) 187.
[32] P. Wu, Y.M. Liu, M.Y. He, M. Iwamoto, Chem. Mater. 17 (2005) 3921.
[33] M. Mamak, N. Coombs, G. Ozin, J. Am. Chem. Soc. 122 (2000) 8932.
[34] M. Mamak, N. Coombs, G. Ozin, Adv. Mater. 12 (2000) 198.
[35] Y.Y. Sun, L. Yuan, S.Q. Ma, Y. Han, L. Zhao, W. Wang, C.L. Chen, F.-S. Xiao, Appl. Catal. A: Gen. 268 (2004) 17.
[36] J. Livage, M. Henry, C. Sanchez, Prog. Solid State Chem. 18 (1988) 259.
[37] Z.Y. Yuan, A. Vantomme, A. Léonard, B.L. Su, Chem. Commun. 13 (2003) 1558.
[38] F. Kleitz, W. Schmidt, F. Schüth, Micropor. Mesopor. Mater. 44–45 (2001) 95.
[39] W.Y. Lin, Q. Cai, W.Q. Pang, Y. Yue, B.S. Zou, Micropor. Mesopor. Mater. 33 (1999) 187.
[40] U. Ciesla, F. Schüth, Micropor. Mesopor. Mater. 27 (1999) 131.
[41] C.T. Kresge, M.E. Leonowicz, W.J. Roth, J.C. Vartuli, J.S. Beck, Nature 359 (1992) 710.
[42] B.T. Holland, P.K. Isbester, C.F. Blanford, E.J. Munson, A. Stein, J. Am. Chem. Soc. 119 (1997) 6796.
[43] R.C.T. Slade, J.C. Southern, I.M. Thomson, J. Mater. Chem. 1 (1991) 563.
[44] L.F. Nazar, G. Fu, A.D. Bain, J. Chem. Soc., Chem. Commun. 20 (1992) 251.
[45] J.S. Xu, Z. Gao, Micropor. Mesopor. Mater. 24 (1998) 213.
[46] E. Rodríguez-Castellón, P. Olivera-Pastor, A. Jiménez-López, J. Sanz, J.L.G. Fierro, J. Phys. Chem. 99 (1995) 1491.
[47] A. Sayari, I. Moudrakovski, J.S. Reddy, C.I. Ratcliffe, J.A. Ripmeester, K.F. Preston, Chem. Mater. 8 (1996) 2080.